

Thermodynamic Atmospheric Profiling During the 2010 Winter Olympics Using Ground-Based Microwave Radiometry

Domenico Cimini, Edwin Campos, Randolph (Stick) Ware, Steve Albers, Graziano Giuliani, Jeos Oreamuno, Paul Joe, Steve E. Koch, Stewart Cober, and Ed Westwater, *Fellow, IEEE*

Abstract—Ground-based microwave radiometer profilers in the 20–60-GHz range operate continuously at numerous sites in different climate regions. Recent work suggests that a 1-D variational (1-DVAR) technique, coupling radiometric observations with outputs from a numerical weather prediction model, may outperform traditional retrieval methods for temperature and humidity profiling. The 1-DVAR technique is applied here to observations from a commercially available microwave radiometer deployed at Whistler, British Columbia, which was operated by Environment Canada to support nowcasting and short-term weather forecast-

ing during the Vancouver 2010 Winter Olympic and Paralympic Winter Games. The analysis period included rain, sleet, and snow events (~ 235 -mm total accumulation and rates up to 18 mm/h). The 1-DVAR method is applied “quasi-operationally,” i.e., as it could have been applied in real time, as no data were culled. The 1-DVAR-achieved accuracy has been evaluated by using simultaneous radiosonde and ceilometer observations as reference. For atmospheric profiling from the surface to 10 km, we obtain retrieval errors within 1.5 K for temperature and 0.5 g/m^3 for water vapor density. The retrieval accuracy for column-integrated water vapor is 0.8 kg/m^2 , with small bias (-0.1 kg/m^2) and excellent correlation (0.96). The retrieval of cloud properties shows a high probability of detection of cloud/no cloud (0.8/0.9, respectively), low false-alarm ratio (0.1), and cloud-base height estimate error within ~ 0.60 km.

Index Terms—Atmospheric measurements, Bayesian variational methods, radiometry.

Manuscript received October 4, 2010; revised March 2, 2011; accepted April 23, 2011. This work was supported in part by Environment Canada, the project Science of Nowcasting Olympic Weather for Vancouver 2010 (SNOW-V10) and in part by the U.S. Department of Energy under Contract DE-AC02-06CH11357. The work of D. Cimini was supported by the Institute of Methodologies for Environmental Analysis (IMAA), Italian National Research Council (CNR).

D. Cimini is with the Institute of Methodologies for Environmental Analysis (IMAA), Italian National Research Council (CNR), 85050 Tito Scalo, Italy. He is also with the Center of Excellence for Severe Weather Forecast (CETEMPS), University of L'Aquila, 67100 L'Aquila, Italy (e-mail: cimini@imaa.cnr.it).

E. Campos is with the Atmospheric Radiation Measurement (ARM) Climate Research Facility, Computing, Environment and Life Sciences Directorate, Argonne National Laboratory, Argonne, IL 60439-4847 USA (e-mail: ecampos@anl.gov).

R. Ware is with Radiometrics Corporation, Boulder, CO 80301 USA. He is also with the National Center for Atmospheric Research, Boulder, CO 80307-3000 USA, and also with the Cooperative Institute for Research in Environmental Sciences, Boulder, CO 80309-0216 USA (e-mail: ware@radiometrics.com).

S. Albers is with the Earth System Research Laboratory, National Oceanic and Atmospheric Administration, Boulder, CO 80305-3328 USA, and also with the Cooperative Institute for Research in the Atmosphere, Fort Collins, CO 80523-1375 USA (e-mail: Steve.Albers@noaa.gov).

G. Giuliani was with the Center of Excellence for Severe Weather Forecast (CETEMPS), University of L'Aquila, 67100 L'Aquila, Italy. He is now with the International Centre for Theoretical Physics, United Nations Educational, Scientific and Cultural Organization, 34151 Trieste, Italy (e-mail: ggiulian@ictp.it).

J. Oreamuno is with Radiometrics Corporation, Boulder, CO 80301 USA (e-mail: jeos@radiometrics.com).

P. Joe and S. Cober are with the Cloud Physics and Severe Weather Research Section (ARMP), Meteorological Research Division, Science and Technology Branch, Environment Canada, Toronto, ON M3H 5T4, Canada (e-mail: paul.joe@ec.gc.ca; stewart.cober@ec.gc.ca).

S. E. Koch is with the National Severe Storms Laboratory, National Oceanic and Atmospheric Administration, Norman, OK 73072 USA (e-mail: Steven.Koch@noaa.gov).

E. Westwater is with the Cooperative Institute for Research in Environmental Sciences, Boulder, CO 80309-0216 USA (e-mail: ed.r.westwater@colorado.edu).

Color versions of one or more of the figures in this paper are available online at <http://ieeexplore.ieee.org>.

Digital Object Identifier 10.1109/TGRS.2011.2154337

I. INTRODUCTION

AUTOMATIC thermodynamic profiles of the lower atmosphere can be continuously retrieved on a minute time scale from a ground-based microwave radiometer profiler (MWRP) working in the 20–60-GHz range. MWRPs are in continuous operation, for research and demonstration, at numerous worldwide sites. Several national and regional meteorological services are now using MWRPs in research and operational modes. There are regions, as for example, in Europe or China, where the MWRP distribution has reached that of radiosonde stations, and similar distribution is likely in other regions soon (India, the U.S., etc.). However, instrumented balloon launches (radiosondes) remain the *de facto* standard for upper air monitoring. Improvements in MWRP data processing are desirable for real operational use of MWRP observations in weather analysis and forecasting (e.g., [1]). Traditional MWRP data processing requires local temperature, humidity, and cloud liquid profile climatology. The climatology is typically derived from radiosonde observations (RAOBs) taken near the radiometer site. The MWRP measurements are then combined with the radiosonde climatology, using statistical inversion techniques [such as neural networks (NNs) or regression methods] to obtain the vertical profiles and the vertically integrated amounts of various atmospheric variables. Recent work [2]–[4], based respectively on a cleaned data set, model data, and research instrumentation, suggests that a 1-D variational (1-DVAR) technique, coupling radiometric observations with

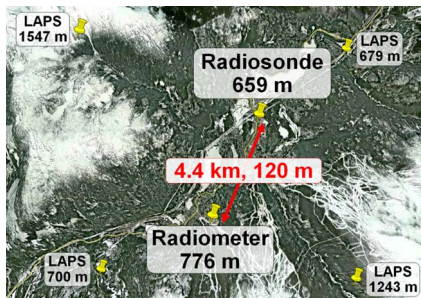


Fig. 1. Radiometer, radiosonde, and LAPS grid point locations and altitudes for this study (north is up). Surface pressure, temperature, and relative humidity comparisons between the radiosonde and radiometer sites give 12.7 mb (0.5 mb), -0.8 K (1.8 K), and 3% (11%) mean (rms) difference, with 1.0, 0.84, and 0.80 correlation coefficients, respectively.

outputs from a numerical weather prediction (NWP) model, is able to outperform other temperature and humidity profiling retrieval methods. This approach avoids the error inherent in NN or regression retrieval methods and benefits from recent surface, radiosonde, satellite, radar, and other data assimilated in the NWP model. Since global NWP data (analysis and/or forecast) are freely available—as from the U.S. National Center Environmental Prediction (NCEP)—the 1-DVAR technique can be adapted to work virtually in any place in the world.

More recently, an NN technique [5] has been applied to observations from an MWRP deployed at the base of the Whistler Creekside Gondola, operated by Environment Canada (EC) (Fig. 1). Its continuous thermodynamic soundings were used in real time by the Meteorological Service of Canada to support nowcasting and short-term weather forecasting during the Vancouver 2010 Olympic and Paralympic Winter Games. The MWRP at Whistler was colocated with other atmospheric observation instruments as part of an international field experiment called SNOW-V10 [6]–[8]. The data set collected during the 2010 Winter Games provides a unique opportunity to advance operational use of continuous thermodynamic profiling by microwave radiometry, with emphasis on the boundary layer. There is consensus that these data are important for improved NWP [9], [10].

This paper expands on previous results [2]–[4] by adding quasi-operational implementation. In here, 1-DVAR retrievals are obtained during all-weather conditions using continuous observations (24 h, 7 days per week) from operational commercially available microwave radiometer. We show the results from zenith and off-zenith NN and 1-DVAR retrievals obtained during 24 days of continuous sampling, covering the 2010 Winter Olympics period. These results include a comparison with simultaneous radiosonde profiles and ceilometer cloud-base estimates in order to quantify the retrieval accuracies.

II. INSTRUMENTS AND METHODS

This paper focuses on the period from 18 UTC February 5 to 12 UTC February 28, 2010. In addition to the MWRP and ceilometer observations at Creekside [50.09° N, 122.98° W, 776 m above sea level (asl)], atmospheric pressure, temperature, and humidity profiles were measured with radiosondes launched by EC from a nearby station, Nesters (50.12° N,

122.95° W, 659 m asl). Atmospheric profiles from the analysis output of the U.S. National Oceanic and Atmospheric Administration (NOAA) Local Analysis and Prediction System (LAPS) were also available for the area surrounding the Creekside and Nesters sites. Fig. 1 shows the location and altitude of instruments and LAPS grid points.

A. Instrumentation

The data used in this paper were collected by continuous MWRP (at near 3-min intervals) and ceilometer observations (at 1-min intervals) and by 94 radiosonde ascents (at 6-h intervals). The MWRP is a Radiometrics MP-3000A unit, including a scanning multichannel microwave radiometer, a one-channel broad-band infrared (IR) radiometer, and surface pressure, temperature, and humidity sensors. The MWRP IR radiometer (9.6 – 11.5 μm) measures sky IR temperature (T_{ir}) and gives information on cloud-base temperature. The MWRP surface meteorology sensors measure temperature (T_s), pressure (P_s), and relative humidity (RH_s). During the period considered here, the MWRP observed brightness temperature (T_b) in 22 channels at two elevation angles (zenith and 15°) and one fixed azimuth angle (northwest in Fig. 1). The channel center frequencies are 22.234, 22.5, 23.034, 23.834, 25.0, 26.234, 28.0, 30.0, 51.248, 51.76, 52.28, 52.804, 53.336, 53.848, 54.4, 54.94, 55.5, 56.02, 56.66, 57.288, 57.964, and 58.8 GHz, with 300-MHz bandwidth. The microwave radiometer is calibrated using noise diode injection to measure the system gain continuously. The noise diode effective temperature is determined by observing an external cryogenic target less frequently (three to six months). The MWRP channels used here were calibrated a couple of months in advance to the Winter Olympics, using an external liquid nitrogen target ($T_b \sim 78$ K) and an internal ambient target ($T_b \sim 278$ K). The calibration period (December 4–5, 2009) was chosen as close as convenient to the Winter Olympics period, due to the access restrictions during and close to the Olympics period. Note that the tipping curve calibration method was not used because the steep topography blocked the upslope view and one-side tipping curve is not recommended (because it may introduce bias induced by leveling errors). On the other hand, thermodynamic retrievals used vertical or off-vertical (15° elevation; downslope) observations. When comparing the zenith with off-zenith results during precipitation, we found that off-zenith observations at 15° are less affected by spurious signals from liquid water accumulated on the radiometer radome.

The ceilometer is a Vaisala CT25K model, which was located a few meters from the MWRP. The ceilometer data used here are the ceiling height measurements provided by the original software; backscatter profiles are not included. The ceilometer data are used only for validating 1-DVAR cloud-base height (CBH) estimates.

Radiosondes launched from the Nesters station are GPS-enabled Vaisala RS92-SGP systems, providing vertical pressure, temperature, relative humidity, dew point temperature, and wind profiles at 2-s resolution. From 18 UTC February 5 to 12 UTC February 28, 2010, four RAOBs were obtained daily at standard synoptic hours (00, 06, 12, and 18 UTC). The

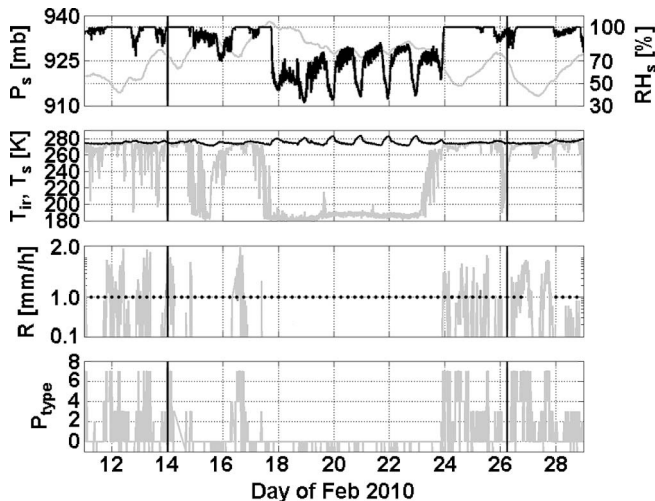


Fig. 2. Ancillary surface measurements, February 11–28, 2010. (Top) (Gray, left axes) Surface pressure (P_s) and (black, right axes) relative humidity (RH_s). (Upper middle) (Black) Surface temperature (T_s) and (gray) sky IR temperature (T_{ir}). (Lower middle) Precipitation rate (R); the black dots indicate the times of radiosonde launch. (Bottom) Precipitation type (–1: no data, 0: no precipitation, 1: precipitation, 2: drizzle, 3: rain, 4: snow, 5: hail, 6: ice crystals, and 7: snow grains or pellets). The vertical black lines indicate the launch times of the two radiosondes in Fig. 3.

RAOB profiles are used for validating 1-DVAR temperature and humidity profiles and were not assimilated into the LAPS NWP model. For comparison, the RAOB relative humidity profiles are converted into water vapor density profiles, using RAOB temperature and pressure. Moreover, RAOB relative humidity was used to estimate cloud liquid profiles by means of the Decker model [11], which is a simple cloud model widely used in propagation and remote sensing simulations. The Decker model identifies cloud layers where the observed relative humidity exceeds a constant threshold, set to 95%, and it associates constant water content to the entire layer, its value depending on cloud thickness only.

The presence and type of precipitation were estimated by a laser-based optical particle size and velocity (Parsivel) disdrometer, located next to the MWRP and ceilometer at Creekside. The Parsivel disdrometer distinguishes different types of precipitation and classifies the particles as drizzle, rain, sleet, hail, snow, or mixed precipitation [12]. The precipitation rate was estimated by an X-band Doppler radar, the Precipitation Occurrence Sensor System [13]. The surface conditions experienced during the Olympic period are shown in Fig. 2. Note that clear sky was detected for a total of 163 h (38% of the period), while precipitation was detected for 92 h (22% of the period). Rain, drizzle, sleet, and snow were detected for 8% (33 h), 2% (7 h), 7% (32 h), and 5% (20 h) of the time period, respectively. Precipitation rates (liquid equivalent) at times exceeded 18 mm/h with about 235-mm total accumulation over the period. Clear sky periods are identified by low T_{ir} temperature, as from day 18 to 23. In Fig. 2, the launch times of Nester radiosondes are also marked; two exemplarily radiosondes representing rainy (00 UTC February 14) and cloudy (06 UTC February 26) weather conditions are indicated with further discussion in Section III.

B. Retrieval Technique

MWRP multichannel observations are commonly used to estimate profiles of temperature and moisture profiles by virtue of multiple probing depths (weighting functions) that the channel set can provide. Because of fundamental ground-based radiometer physics, derived profile vertical resolution and accuracy decrease with increasing altitude. Traditionally, MWRP retrievals use linear (e.g., regression), nonlinear (e.g., iterative), or NN methods [5], partially overcoming the lack of sensitivity at the higher levels by incorporating statistical correlations between lower and higher levels. The use of proper background data and vertical statistics is vital for achieving the highest accuracy. Recent results [2]–[4] show that coupling the radiometer data with the output of a numerical model analysis or forecast through 1-DVAR can improve the retrieval accuracy over either linear or NN method alone. The 1-DVAR method combines observed and forward-modeled brightness temperatures with model covariance matrices to optimize retrieval accuracy. Temperature and humidity retrieval accuracy in the upper troposphere depend primarily on the model analysis, and those in the boundary layer and lower troposphere depend primarily on the radiometer. Thus, the 1-DVAR approach avoids the error inherent in methods initialized with local climatology (as for NN and regression) and benefits from recent surface, radiosonde, satellite, radar, and other data assimilated in the local analysis or forecast.

The details of the 1-DVAR implementation used here are given in [4]. The iterative solution that minimizes a cost function J is given by

$$\mathbf{x}_{i+1} = \mathbf{x}_i + \left((1 + \gamma)\mathbf{B}^{-1} + \mathbf{K}_i^T \mathbf{R}^{-1} \mathbf{K}_i \right)^{-1} \cdot \left[\mathbf{K}_i^T \mathbf{R}^{-1} (\mathbf{y} - F(\mathbf{x}_i)) - \mathbf{B}^{-1} (\mathbf{x}_i - \mathbf{x}_b) \right] \quad (1)$$

where \mathbf{x}_i and \mathbf{x}_b are the current and background state vectors, respectively; \mathbf{B} and \mathbf{R} are the error-covariance matrices of the background and observation vector \mathbf{y} , respectively; $F(\mathbf{x})$ is the forward model operator; \mathbf{K} is the Jacobian matrix of the observation vector with respect to the state vector; and γ is the Levenberg–Marquardt factor. Note that the 1-DVAR method allows quantification of the retrieval performance by propagating statistical errors from both observations and background. As explained in [14], the expected error profile is given by the diagonal terms of

$$\mathbf{A}_i = \left(\mathbf{B}^{-1} + \mathbf{K}_i^T \mathbf{R}^{-1} \mathbf{K}_i \right)^{-1}. \quad (2)$$

Details on the settings of the 1-DVAR present implementation are given in the next section.

C. Settings

With respect to previous implementations [2]–[4], the novel aspect of this work is the quasi-operational application; in fact, 1-DVAR retrievals were obtained during all-weather conditions using observations from a 24/7 operational commercially available microwave radiometer. The background information in (1) comes from NOAA LAPS [15] analyses. In particular, we use the atmospheric profiles extracted from LAPS analysis at the

grid point nearest to the MWRP site, namely, the southwest corner in Fig. 1 (50.07° N, 123.05° W, 700 m asl). We run here a 2010 version of the LAPS, generating a new set of analyses every hour, at a 10-km horizontal grid and a vertical resolution of 25 mb on a constant pressure grid. LAPS collects satellite, airplanes, wind profilers, Doppler radar, and RAOB observations, performing smooth blending with background first guess and 3-D weighting. More details on LAPS data assimilation are given in [9]. The RAOB closest to Whistler that is assimilated into LAPS at 00Z and 12Z comes from Quillayute, WA, at some 400-km distance. To simulate 1-DVAR real-time operational conditions, we consider the delay for LAPS output delivery. Since the analysis usually finishes by about 30–40 min after the nominal analysis time, we use the analysis at nominal time at least 50 min before the MWRP observations as background. Note that the LAPS runs did not assimilate any of the data that we use later in Section III for validation (i.e., ceilometer or radiosonde). The state vector \mathbf{x}_i in (1) consists of profiles of temperature (T) and the natural logarithm of the total water (Q), i.e., the total of specific humidity and condensed water content. The choice of $\ln Q$ as state vector has the following advantages: reduced state vector dimension, implicit correlation between humidity and condensed water, error characteristics that are more closely Gaussian, and prevention of unphysical retrieval of negative humidity [3], [4]. The total water is initialized using LAPS humidity, cloud liquid, and ice water, while other hydrometeors (such as rain, snow, and graupel) are not used. The state vectors are given on the same 81 vertical levels defined for the LAPS model, although we perform retrievals just for 0- to 10-km levels. The observation vector in (1) is given by MWRP Tbs at 15° elevation angle, as well as by the MWRP surface pressure, temperature, and humidity readings.

Estimates of the background and observation error-covariance matrices (\mathbf{B} and \mathbf{R} in (1), respectively) were obtained by using a set of LAPS profiles, radiosonde ascents, and MWRP ground-based observations. The observation error-covariance matrix \mathbf{R} was estimated for the MWRP data following the approach in [3] and [4]. Note that radiometric noise, calibration, representativeness, and forward model errors all contribute to the observation error covariance \mathbf{R} . The background error-covariance matrices \mathbf{B} for both temperature and humidity profiles were computed from a set of simultaneous LAPS and RAOB data (both in clear and cloudy weather conditions), collected at the same model grid point and radiosonde launch site as before, but for the period from 00 UTC March 6 to 12 UTC March 21, 2010. Thus, the error-covariance period does not overlap the analysis period, although the weather conditions in the region are similar in February and March. This calculation of \mathbf{B} inherently includes forecast errors, as well as instrumental and representativeness errors from the radiosondes (i.e., errors associated with representation of a volume by point measurements). However, a \mathbf{B} matrix including these terms seems appropriate for the radiometric retrieval minimization, since the grid cell of the NWP model is much larger than the radiometer observation volume. Similar to RAOBs, the radiometer observations can be assumed as a point measurement when compared to the model cell. Values for the estimated \mathbf{B} and \mathbf{R} were found to be consistent with those in

[4] and were given elsewhere [16]. Note that, in general, the 1-DVAR retrieval skill depends on how well the estimated \mathbf{B} and \mathbf{R} represent reality. In a future operational deployment, \mathbf{B} and \mathbf{R} may be changed dynamically (e.g., periodically and conditionally) to account for changes in instrument and meteorological conditions, thus improving the retrieval accuracy.

The forward model $F(\mathbf{x})$ used here is the NOAA microwave radiative transfer code [17], which also provides the weighting functions that we use to compute the Jacobians \mathbf{K} with respect to temperature and total water. The adopted forward model does not cover the IR spectrum, and thus, observations from the broad-band IR radiometer were not included in observation vector. Note also that scattering signal is considered negligible (i.e., within the instrumental error). For the frequencies considered here (< 60 GHz), this approximation is valid also in the presence of snow, as recently demonstrated [18]. Brightness temperatures at the MWRP central frequencies are forward modeled from temperature, water vapor, and liquid water profiles. Errors with respect to band-averaged Tb —including spectral filter characteristics—are typically within 0.1 K, and these were accounted for in the forward modeling component of the observation error. The observations-minus-simulations bias was investigated for each MWRP microwave channel at 15° elevation and was found to range from 1.5 K to 3.0 K for the K-band channels (i.e., 22–30 GHz), from 0.9 K to 1.9 K for lower V-band channels (i.e., 51–53 GHz), and from 0.0 K to 0.5 K for the higher V-band channels (i.e., 53–59 GHz), showing no evidence of trend over time. The source of these biases can be attributed to radiometer calibration uncertainty, gas absorption model [19], radiosonde bias error [20], and radiometer–radiosonde collocation error. In addition, for radiometer observations at 15° elevation, small (0.1°) leveling error can generate several-degrees-kelvin brightness temperature error in the K-band and lower V-band.

Special attention was dedicated to the 1-DVAR optimization for operational use. The Levenberg–Marquardt factor γ is adjusted after each iteration, depending on how the cost function J has changed. If J has increased, γ is increased by a factor of ten, and the iteration is repeated; if J has decreased, γ is decreased by a factor of two for the next iteration. These factors were suggested in [3] and the references therein. Moreover, the 1-DVAR technique is applied in two steps, because this approach was found to improve the convergence efficiency. The steps are as follows.

- 1) The temperature profile is retrieved from a selection of V-band channels, corresponding to the nine higher frequency channels (53.848, 54.4, 54.94, 55.5, 56.02, 56.66, 57.288, 57.964, and 58.8 GHz). These channels were selected because they are less sensitive to cloud water and rain. The convergence criterion described in [21] was adopted, leading to successful convergence, usually within three iterations.
- 2) The retrieved temperature profile is set as background, and the natural logarithm of total water is retrieved from the complete set of K-band channels. The iteration is stopped when the profile increment has decreased by less than 10%, leading to convergence, usually within

nine iterations. The retrieved total water is partitioned between specific humidity and condensed water (see in the following). The specific humidity is then converted into water vapor density for comparison purposes, using retrieved temperature and background pressure.

Note that the liquid water content (L) is inherently estimated in our 1-DVAR implementation from the adopted state vector, i.e., the natural logarithm of the total water. Using the approach in [3] and [4], the retrieved total water is partitioned at each iteration step between specific humidity and condensed water content. The condensed water is further partitioned between liquid and ice fractions, assuming a linear dependence on air temperature, and the ice fraction is ignored as it is assumed to have negligible extinction for the MWRP channels [4]. Note that, in the current 1-DVAR implementation, the T_{ir} observations are not used and the cloud boundaries and liquid water content are initially set to the values given by the LAPS background.

D. Other Retrieval Techniques

The 1-DVAR retrievals are compared hereinafter with LAPS and RAOB profiles, as well as with NN retrievals. The NN retrievals used here are generated by the MP-3000A proprietary software [5]. Five years of historical operational radiosondes from Kelowna (49.93° N, 119.40° W, 456 m asl, and ~250-km distance from Whistler) were adjusted to the radiometer site altitude and processed to generate thousands of synthetic liquid water content profiles. Radiosonde plus liquid water profiles were processed within a radiative transfer model and used as the NN training set. The NN retrievals are computed by using two versions of the proprietary software, one ingesting zenith observations (NNz) and the other ingesting slant observations at 15° elevation (NNs). NNs and NNz estimate separately and in parallel the temperature, water vapor density, relative humidity, and liquid water content profiles from all K- and V-band channels plus the IR channel. The only difference between NNs and NNz is the observing elevation angle (15° and 90°, respectively). NNz and NNs retrievals were obtained in real time, and no data were culled even in the presence of rain, sleet, or snow. Note that NNs and 1-DVAR retrievals are based on the same MWRP observations, with the following exceptions.

- 1) The 1-DVAR retrievals do not use the IR thermometer observations.
- 2) For the 1-DVAR retrievals, a constant value for each MWRP channel has been removed to the observed T_b . The impact of this bias correction is discussed in Section IV.

E. Skill Scores

Conventional skill scores for meteorology have been defined in [22]. Similar to those, the score indexes used in Section III to quantify the performances of cloud detection are adapted from [23]. Using the notation in Table I for indicating the number of cases in which cloud or no cloud was observed by the ceilometer and estimated by the various methods, the formulations of the following skill score indexes for cloud detection are given in Table II: probability of detection of cloud

TABLE I
CONTINGENCY TABLE FOR THE EVALUATION OF CLOUD AND NO-CLOUD DETECTIONS (TO BE USED WITH TABLE II EQUATIONS)

Observed → Estimated ↓	Cloud	No-Cloud
Cloud	n_{CC}	n_{NC}
No-cloud	n_{CN}	n_{NN}

TABLE II
SCORE INDEXES FOR CLOUD DETECTION USED TO EVALUATE THE DETECTION CAPABILITY OF A PARTICULAR METHOD WITH RESPECT TO CEILOMETER ESTIMATES. THE TABLE INCLUDES THE WORST AND BEST VALUES FOR EACH INDEX (TO BE USED WITH THE DEFINITIONS IN TABLE I)

Score Index	Expression	Worst Value	Best Value
PODN	$\frac{n_{NN}}{n_{NC} + n_{NN}}$	0	1
PODC	$\frac{n_{CC}}{n_{CN} + n_{CC}}$	0	1
FAR	$\frac{n_{NC}}{n_{CC} + n_{NC}}$	1	0

(PODC), probability of detection of no cloud (PODN), and false-alarm ratio (FAR).

III. RESULTS

The 1-DVAR method, with the implementation described earlier, was applied to the MWRP observations on February 5–28, 2010, including the 2010 Winter Olympics period. The weather conditions encountered during this period are summarized in Fig. 2: Clear and cloudy sky periods were detected, as well as different kinds of precipitation. We emphasize that the 1-DVAR retrievals were obtained in offline postprocessing, but the results shown below are “quasi-operational” in the sense that they would have been the same if processed online because the method is fast enough to be implemented in quasi-real time and no data were culled in the processing. With the convergence criteria introduced earlier, the convergence rate for the period under analysis was 100% for temperature and 99.5% for total water retrievals. Concerning the computing time, each iteration takes about 0.3 s on a Linux personal computer with 2-GHz CPU and 2-GB RAM. Considering an average of three iterations for temperature and nine for total water profiles, a complete retrieval is available in less than 4 s.

In the following, 1-DVAR and NN retrievals are compared with LAPS and RAOB profiles. From the total of 94 RAOBs available, our analysis is based on 72 cases in which all the data sources (RAOB, LAPS, and MWRP) were simultaneously available. These 72 cases include clear, cloudy, and precipitation weather conditions. Fig. 3 shows two cases with (A and B) temperature, (C and D) humidity, and (E and F) cloud liquid profiles as provided by RAOB, LAPS, and MWRP retrievals (NN and 1-DVAR). These cases were selected as representatives of rainy [00 UTC February 14; Fig. 3(a), (c), and (e)] and cloudy [06 UTC February 26; Fig. 3(b), (d), and (f)] weather condition periods.

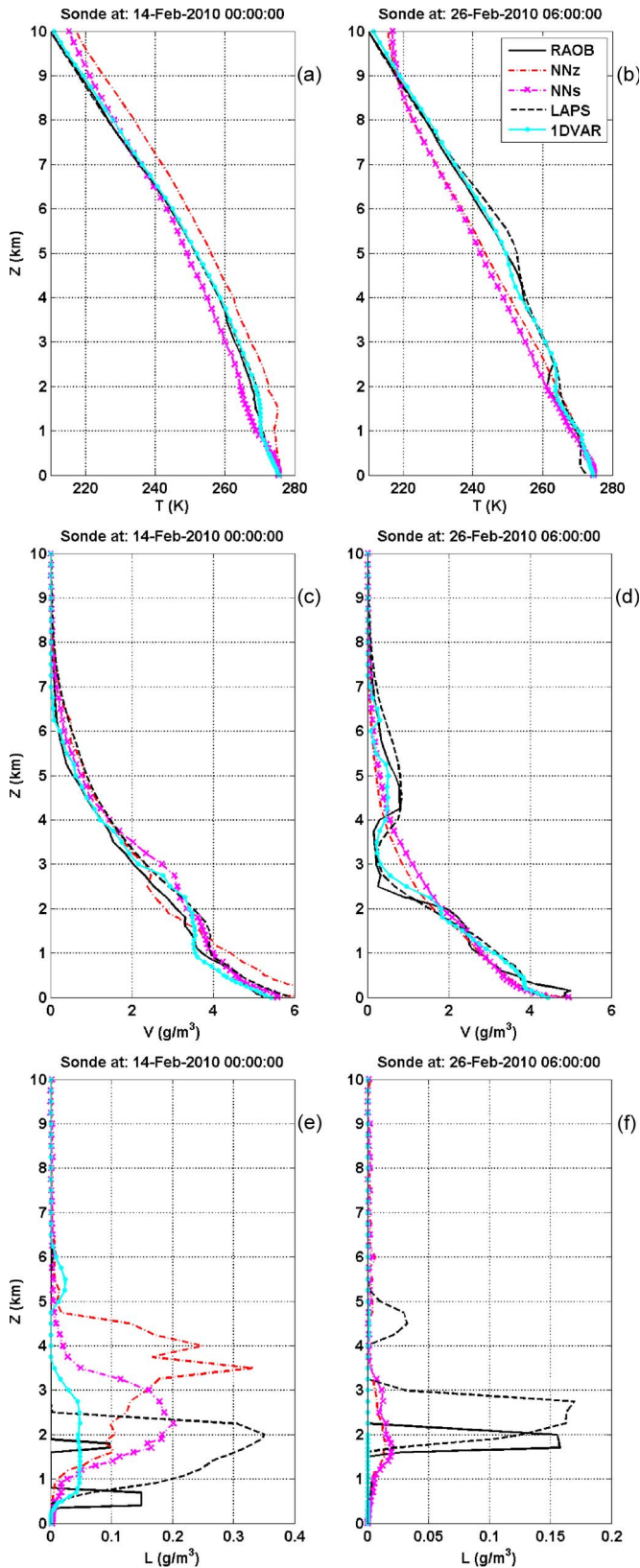


Fig. 3. Selected profiles of (top; A and B) temperature, (middle; C and D) water vapor density, and (bottom; E and F) cloud liquid water as provided by RAOB, LAPS, NNz and NNs retrievals, and 1-DVAR retrievals. The vertical axis Z indicates the height above the MWRP level. (Left; A, C, and E) Case with rain precipitation ($R \sim 4\text{--}7$ mm/h; $T_{ir} = 274.5$ K). (Right; B, D, and F) Case with clouds but no precipitation ($T_{ir} = 246.4$ K). The legend in the upper right panel indicates the line color/style coding.

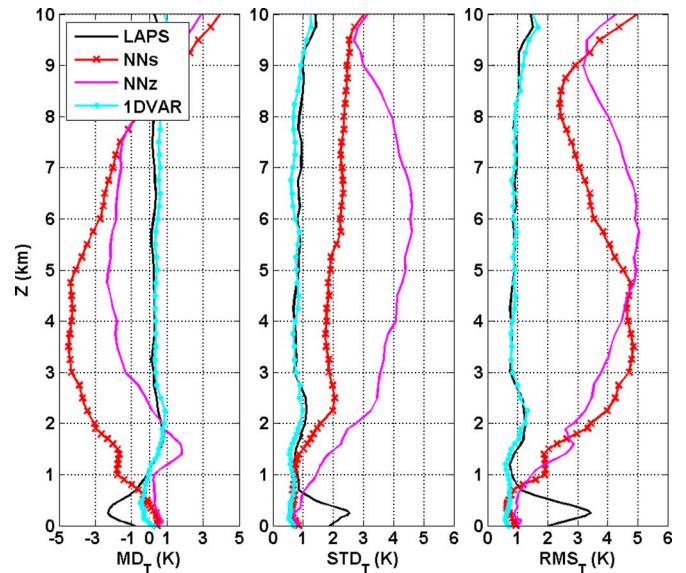


Fig. 4. Comparison of LAPS, NNs , NNz , and 1-DVAR temperature profiling accuracies with respect to RAOB (72 cases). (Left) MDs (RAOB minus retrievals or simulations). (Center) STD difference. (Right) RMS difference. The legend in the top-left corner indicates the line color/style coding.

A. Temperature Profiles

The individual temperature profiles in Fig. 3(a) and (b) show that both the LAPS analyses and the MWRP retrievals follow the temperature vertical structure measured by the RAOB. For the case with rain precipitation (00 UTC February 14), NNz retrievals differ largely from the other MWRP retrievals and from RAOB. This difference is attributable to the fact that NNz retrievals rely on zenith observations, which are affected by rain accumulating over the radome. Conversely, NNs and 1-DVAR both rely on 15° elevation observations and thus mitigate substantially the impact of rain residual. For the cloudy case (06 UTC February 26), the NNz and NNs retrievals match well the RAOB temperature profile in the boundary layer but show significantly larger differences in the upper atmosphere. This result is consistent with the weighting function of V-band channels, peaking near the surface and fading rapidly above the lower few kilometers [24]. Conversely, the LAPS analyses represent well the RAOB temperature structure up to 10 km in both cases, although presenting larger differences near the surface in one of the two cases. This is consistent with the estimated background error B (not shown), which indicates small values for temperature background error above 1-km altitude but much larger values in the boundary layer. The 1-DVAR retrievals, being an optimal combination of ground-based observations and background information, retain the information carried by the background LAPS temperature analyses, particularly in the upper troposphere, while being able to correct inaccurate LAPS analyses in the lower few kilometers. The combination of these two features allows the 1-DVAR to achieve the best retrieval performances throughout the vertical domain. This is demonstrated in Fig. 4, which shows the mean difference (MD), standard deviation (STD), and root-mean-square (rms) difference for simultaneous temperature profiles (from LAPS, NNs , NNz , and 1-DVAR),

using RAOB as the reference. If one assumes that RAOB provides true and representative temperature profiles for MWRP observations, then the 1-DVAR retrieval accuracy—in term of rms—is within 1.5 K for heights up to 10 km above ground. Under this assumption, the 1-DVAR shows the best retrieval accuracy, which is comparable to the accuracy of NN in the boundary layer and to the accuracy of LAPS analysis in the upper atmosphere up to nearly the tropopause.

B. Water Vapor Profiles

The water vapor density (V) profiles in Fig. 3(c) and (d) (middle panels) show that both the LAPS analyses and the MWRP retrievals follow the humidity vertical structure measured by the RAOB. In particular, the LAPS analyses seem to carry more information about the vertical distribution of water vapor and therefore catch the presence of elevated humidity inversions. As with temperature, the agreement between RAOB and LAPS vapor densities is less near the surface than in the upper atmosphere as a result of a multitude of local boundary-layer conditions induced by the complex terrain, which cannot be resolved in the LAPS analyses. In contrast, the retrievals based on MWRP observations are in better agreement with RAOB in the lower atmosphere, probably because of the constraint given by the MWRP surface measurements. However, MWRP retrievals usually miss details in the vertical structure because of the smooth quasi-constant weighting functions at K-band frequencies [24]. Similar to temperature, Fig. 3(c) and (d) shows that the 1-DVAR humidity retrievals are able to retain the information carried by the background LAPS analysis, particularly in the upper troposphere. The 1-DVAR retrievals are also able to correct the LAPS analysis in the lower few kilometers. The statistics of humidity retrievals are summarized in Fig. 5, showing the mean, STD, and rms differences for simultaneous water vapor profiles (from LAPS, NNs , NNz , and 1-DVAR), using RAOB as the reference. The same 72 cases described earlier were considered in the analysis. In terms of rms with respect to RAOB, the smallest values are given by NNs , which are $\sim 0.4 \text{ g/m}^3$ from the surface up to 3 km and then decrease aloft almost linearly with height by $0.1 \text{ (g/m}^3\text{)/km}$. NNz , 1-DVAR, and LAPS humidity profiles show rms differences similar to NNs , except near the surface where LAPS rms differences are $\sim 0.8 \text{ g/m}^3$ while NNz and 1-DVAR are $\sim 0.5 \text{ g/m}^3$, all reaching 0.4 g/m^3 at 1 km. Note that NNs and 1-DVAR retrievals are based on 15° observations, but unlike 1-DVAR, NNs water vapor retrievals use both K- and V-band channels. Thus, the correlation between low-level temperature and humidity may explain better NNs performances below 1 km. Above 1 km, LAPS, 1-DVAR, and NN perform nearly the same. These results demonstrate once again that, with respect to LAPS analysis, the MWRP observations provide useful information mainly in the boundary layer, where LAPS shows the largest difference with respect to RAOB due to locally induced meteorological effects.

Microwave radiometer observations at K-band channels are widely used for the retrieval of the integrated water vapor (IWV) content in the atmosphere [24]. Therefore, in Table III,

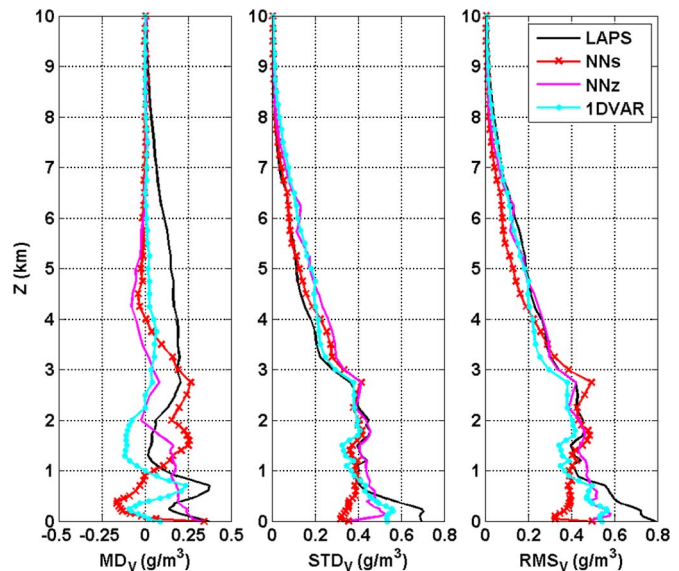


Fig. 5. Comparison of LAPS, NNs , NNz , and 1-DVAR water vapor density profiling accuracies with respect to RAOB (72 cases). (Left) MDs (RAOB minus retrievals or simulations). (Center) STD difference. (Right) RMS difference. The legend in the top-right corner indicates the line color/style coding.

TABLE III
COMPARISON OF IWV ESTIMATES WITH VALUES OBTAINED FROM RADIOSONDES. MD, STD, RMS DIFFERENCE, CORRELATION COEFFICIENT (COR), ESTIMATED STATISTICAL ERROR (SDE), SLOPE (SLP), AND OFFSET (OFS) OF A LINEAR FIT ARE INCLUDED. SEVENTY-TWO CASES WERE USED. (*) THE VALUES ARE IN KILOGRAMS PER SQUARE METER

	LAPS	NNz	NNs	1DVAR
MD (*)	-1.1	-0.2	-0.2	-0.1
STD (*)	0.9	0.9	0.9	0.8
RMS (*)	1.4	1.0	1.0	0.8
COR	0.95	0.93	0.93	0.96
SDE (*)	0.9	0.9	0.9	0.6
SLP	1.0	0.9	0.9	0.8
OFS (*)	0.8	1.0	1.0	2.1

we compare IWV values computed from LAPS and retrieved from NNs , NNz , and 1-DVAR, with the corresponding IWV values computed from RAOB humidity profiles. Table III includes the MD, STD, and rms, as well as the correlation coefficient (COR), the estimated statistical error (SDE), and the slope (SLP) and offset (OFS) of a linear fit. Adopting RAOB as reference, 1-DVAR shows the best accuracy for the IWV range under analysis in terms of the highest correlation coefficient (0.96) and the smallest mean (-0.1 kg/m^2), STD (0.8 kg/m^2), and rms (0.8 kg/m^2) differences with respect to RAOB. However, we acknowledge that the SLP and OFS for the implemented 1-DVAR (including options for **B** and **R**) are the farther from the perfect match (one and zero, respectively). This implies that the 1-DVAR retrieval is optimized for the IWV range under study and it will need to be adapted in different IWV climatologies.

C. Cloud Liquid Profiles

The profiles of cloud liquid water content in Fig. 3(e) and (f) deserve careful explanation. It is anticipated that the accuracy of these liquid profiles may not be adequate for microphysical studies, but here, it is assumed to be adequate for nowcasting purposes. In fact, cloud liquid is not measured by operational meteorological radiosondes such as the RS92 launched at Nesters, and its estimate from ground-based microwave observation alone is limited by lack of degrees of freedom (i.e., vertical resolution) in microwave signals [25]. However, it is recognized that accurate estimates of the vertically integrated liquid water path (LWP) are retrieved from MWRP observations, providing spatial and temporal constraints on the liquid profile. Moreover, the zenith IR observations provide information on cloud-base temperature and height. With these considerations, Fig. 3(e) and (f) provides cloud liquid profiles from (a) LAPS output, (b) NN_s , NN_z , and 1-DVAR retrievals, and (c) indirect derivation from RAOB. These profiles are obtained as follows.

- 1) For the LAPS profiles, the nonprecipitating liquid water content is produced within LAPS from the 3-D analyzed cloud field by using an adiabatic parcel model [15].
- 2) For the 1-DVAR profiles, the cloud structure is initialized with LAPS background and is inherently present in the state vector throughout the retrieval process. Conversely, NN_s and NN_z estimate cloud liquid profiles directly from MWRP microwave and IR channels. Therefore, 1-DVAR, NN_s , and NN_z methods all ingest independent information on cloud vertical structure other than microwave observations alone (LAPS background in 1-DVAR; IR cloud-base temperature in NN_s/NN_z). Nonetheless, even with *a priori* knowledge of cloud boundaries, the vertical distribution of liquid water within the cloud layer is difficult to retrieve from standard MWRP observations, as demonstrated in [25].
- 3) Liquid profiles from RAOB were obtained using the Decker model. This model has been validated against ground-based microwave radiometer and ceilometer observations [26] and was found to be robust enough for LWP and CBH estimations. However, cloud determination from relative humidity profiles is generally problematic. When compared with other meteorological fields, relative humidity shows much more variation in space and time and, thus, smaller representativeness. Cloud liquid water fields are even more variable than relative humidity fields. Therefore, inherent uncertainties and nonrepresentativeness in the relative humidity field can lead to large scatter between the observed relative humidity and cloud presence [25].

Having these considerations in mind, Fig. 3(e) and (f) shows that 1-DVAR and NN retrievals provide realistic cloud boundaries and liquid water content even in the presence of rain [Fig. 3(e)]. Note that ground-based microwave radiometry cannot reliably discriminate between rain and cloud water, unless polarized channels are used ([27] and the references therein), so the retrieved cloud liquid water during rainy conditions may be affected by some rain water contamination. However, the case

TABLE IV
STATISTICS OF CBH WITH RESPECT TO CEILOMETER MEASUREMENTS.
CLOUD DETECTION SCORES ARE PODC, PODN, AND FAR.
ONE-HUNDRED SIXTY-FOUR CASES WERE USED.
(*) VALUES ARE IN KILOMETERS

	LAPS	NNz	NNs	1DVAR
PODC	0.9	0.8	0.8	0.8
PODN	0.8	1.0	1.0	0.9
FAR	0.1	0.0	0.0	0.1
COR	0.70	0.69	0.74	0.70
MD (*)	0.16	-0.81	-0.39	0.16
STD (*)	0.57	0.82	0.70	0.57
RMS (*)	0.60	1.15	0.80	0.60

in Fig. 3(e) shows that both 1-DVAR and NN place the cloud base at some 400-m altitude effectively, where the humidity approaches saturation, as demonstrated by the L profile estimated from the RAOB with the Decker model. For the cloudy case [Fig. 3(f)], LAPS and RAOB both place a liquid cloud from 1.5 km aloft, while NN_s and NN_z show little liquid and 1-DVAR shows no liquid at all. The 1-DVAR estimate is supported by the sky IR temperature ($T_{ir} \sim 246$ K), which indicates that the cloud is likely formed by ice water only.

A reference measurement for liquid water content profile was not available during the period under analysis. In fact, although radar observations were made in the Whistler region during the period analyzed here, liquid water retrievals from C-band radars carry information about large precipitating drops and lack sensitivity to small nonprecipitating droplets forming clouds. As a result, radar observations—of sufficient quality to generate meaningful liquid water retrievals—were not available to us at the time this work was prepared. On the other hand, accurate measurements of CBH were provided by a ceilometer colocated with the MWRP; CBH can also be extracted from liquid water profiles as the height of the lowest level where liquid water content is greater than zero. Therefore, in Table IV, we present the analysis of cloud detection and CBH from cloud liquid profiles by LAPS, NN_s , NN_z , and 1-DVAR, assuming the ceilometer estimates as the reference. Ceilometer data are available at 1-min resolution, and CBH is estimated as the minimum height detected within the observation interval. For that, the MWRP and ceilometer cloud-base estimates were averaged in 10-min windows, centered at the LAPS hourly-analysis times. This averaging resulted in 164 cases where all the data sources (ceilometer, MWRP, and LAPS) were available, including both clear and cloudy weather conditions. Note that there may be ceilometer detections caused by pure ice clouds, which are ignored in the 1-DVAR process. Part of these cases were removed by assuming -40 °C as the limit for liquid water presence (roughly corresponding to 6 km) and thus purging ceilometer CBH > 6 km. Table IV reports the scores for cloud detection skills, as well as for CBH quantitative estimation. According to Table IV, LAPS provides the best PODC but the worst PODN and FAR, suggesting a tendency to overestimate the cloud presence. With regard to quantitative estimation, LAPS and 1-DVAR provide the best accuracy for CBH retrievals in terms of both the correlation coefficient

(0.70), and the mean (0.16 km) and rms (0.60 km) differences. Clearly, the 1-DVAR results do not add significant improvement to the CBH given by LAPS; the cloud boundary information residing in the LAPS background and initially ingested into the 1-DVAR is generally left nearly unchanged during the 1-DVAR iterative process. That is, 1-DVAR produces liquid water profiles that benefit from the LAPS cloud boundary information but, in addition, are consistent with both the measured T_b (leading to more accurate integrated content) and the retrieved temperature and total water profiles.

IV. DISCUSSION AND CONCLUSION

This paper has presented a 1-DVAR technique for temperature, humidity, and cloud liquid profile retrievals from ground-based radiometric observations. The technique was tested during a 24-day period, including the Vancouver 2010 Olympic Winter Games. These 1-DVAR retrievals have been compared with the MWRP NN retrievals, nearby RAOBs, collocated ceilometer observations, and objective analyses from an NWP model. The results tend to confirm that the 1-DVAR technique, being an optimal combination of ground-based observations (from the MWRP) and background information (from objective analyses), outperforms the background initialization, as well as other inversion methods (NN retrievals).

The achieved accuracy has been evaluated assuming that simultaneous radiosonde and ceilometer observations are representatives of the radiometer sampling volume. When comparing 1-DVAR retrievals with radiosonde profiles up to 10 km, we obtained an rms difference within 1.5 K for temperature and within 0.5 g/m^3 for water vapor density. If these 1-DVAR-versus-RAOB differences are considered as the retrieval error, then they correspond to a reduction of 50%–65% (0%–50%) of the temperature (vapor density) field variability, considered as the STD of the entire radiosonde sample (see Fig. 5). Note that, limiting the analysis to clear sky only, we did not notice a clear improvement either in 1-DVAR temperature or humidity retrievals. However, we expect retrieval performances to change with weather conditions. In principle, for nowcasting and data assimilation purposes, as well as other applications, it is desirable to provide an error to each individual retrieved profile. The 1-DVAR expected error profile [i.e., (2)] can be adopted for this purpose; for example, the expected error for water vapor profiles is given in Fig. 6, which indeed suggests the degradation of retrieval performances from clear sky (February 17–24) to dynamical (February 11–16 and 24–28) weather conditions. Quantitative comparison of retrieval accuracy during clear, cloudy, and precipitating conditions is desirable, but it requires an extended data set (one year minimum) to be statistically meaningful. Such a data set would also be useful to refine covariance matrices during dynamical weather conditions. Note also that the 1-DVAR retrieval error is fairly insensitive to the T_b bias correction introduced in Section III. This can be appreciated in Fig. 7, where 1-DVAR rms profiles with and without bias correction are plotted for both temperature and vapor density. However, we acknowledge that the bias correction would have had larger impact if the lower frequency V-band channels were included in the 1-DVAR observation

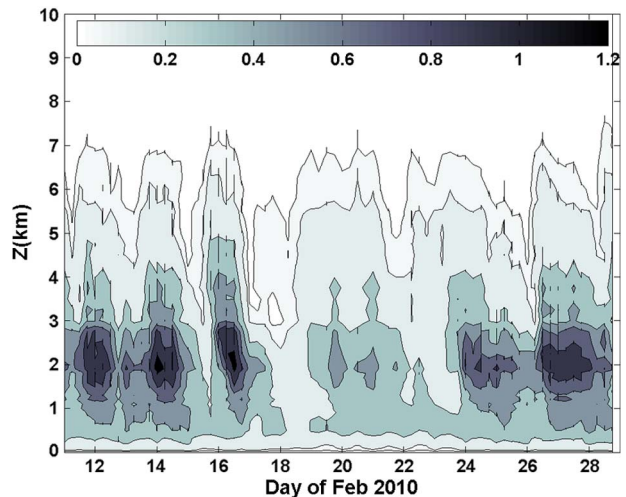


Fig. 6. Contour of time–height cross section of the estimated statistical error for water vapor density retrievals. The values are in grams per cubic meter. The period shown is the same as that in Fig. 2, i.e., clear sky is from February 18 to 24, while precipitation is detected in the February 11–14, 16–17, and 24–28 periods.

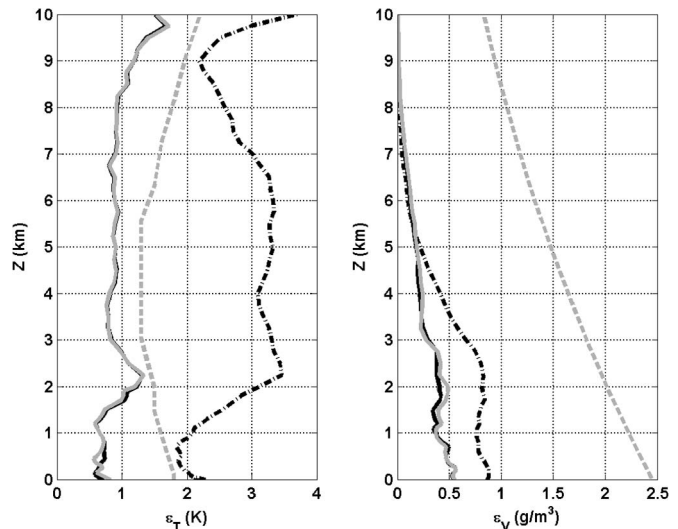


Fig. 7. Errors for temperature and water vapor density estimates. The dashed gray lines correspond to observation errors designated by NCEP to RAOB data assimilation. The solid black (gray) lines correspond to the 1-DVAR retrieval accuracy (rms difference with respect to RAOB) as obtained with (without) T_b bias correction. The dashed–dotted black lines show the variability for RAOB observations of temperature and water vapor density in terms of STD during the study period (72 RAOB profiles).

vector. Fig. 7 also shows the observation errors associated by NCEP to the RAOBs assimilated in the NCEP analysis and forecast models [28], [29]. Note that NCEP observation errors are larger than the 1-DVAR retrieval errors throughout the vertical range from the surface up to 10-km height. The water vapor burden obtained by integrating the retrieved water vapor profiles showed an rms accuracy (assuming RAOB as the reference) within 0.8 kg/m^2 , with small bias (-0.1 kg/m^2) and excellent correlation (0.96). The 1-DVAR rms error corresponds to $\sim 9\%$ of the average IWV, with $\sim 43\%$ improvement with respect to the NWP background, and to $\sim 67\%$ reduction of the IWV field variability.

Unfortunately, no reference measurement was available for the cloud liquid water content or integrated cloud liquid path. Therefore, we do not attempt the estimate of the 1-DVAR retrieval accuracy for either liquid water profiles or integrated amounts. Conversely, cloud detection and base height estimates were validated by using ceilometer data as reference. The results indicate that 1-DVAR provides high PODC/PODN (0.8/0.9, respectively) and low FAR (0.1), with an rms error of ~ 0.60 km, although most of the CBH information comes from the LAPS background.

Finally, considering that the rms errors in Fig. 7 include radiosonde sensor and flight path drift errors, we conclude that the retrievals based on MWRP (1012VAR, as well as NN) are better than 1 K in the first kilometer. Noteworthy, this result is obtained for real-time operations, because no data were culled during rain, sleet, and snow events. Such accuracy in capturing boundary layer and lower tropospheric thermodynamic effects is critical to improving local short-term forecast accuracy, for example, for managing high-profile outdoor sporting events, aviation weather, air quality, fire weather, hazardous airborne material dispersion, and renewable (wind and solar) energy management.

ACKNOWLEDGMENT

The authors would like to thank I. Heckman of Environment Canada (EC) for providing the access to the SNOW-V10 data archive. The radiosonde, ceilometer, and radiometer data are all part of this archive. The author E. Campos would like to thank C. Doyle, Dr. G. Isaac, and M. Harwood of EC for their logistics and planning efforts, who facilitated microwave radiometer installation, calibration, and data collection during his former affiliation with EC.

REFERENCES

- [1] D. A. M. Engelbart, W. A. Monna, J. Nash, and C. Matzler, "Integrated ground-based remote sensing stations for atmospheric profiling," *Earth Syst. Sci. Environ. Manage. (ESSEM)*, Brussels, Belgium, COST Action 720-Final Rep., 2009, 422 pp.
- [2] D. Cimini, T. J. Hewison, L. Martin, J. Guldner, C. Gaffard, and F. Marzano, "Temperature and humidity profile retrievals from ground-based microwave radiometers during TUC," *Meteorol. Zeitschrift*, vol. 15, no. 5, pp. 45–56, Feb. 2006.
- [3] T. Hewison, "1D-VAR retrievals of temperature and humidity profiles from a ground-based microwave radiometer," *IEEE Trans. Geosci. Remote Sens.*, vol. 45, no. 7, pp. 2163–2168, Jul. 2007.
- [4] D. Cimini, E. R. Westwater, and A. J. Gasiewski, "Temperature and humidity profiling in the Arctic using millimeter-wave radiometry and 1DVAR," *IEEE Trans. Geosci. Remote Sens.*, vol. 48, no. 3, pp. 1381–1388, Mar. 2009, doi: 10.1109/TGRS.2009.2030500.
- [5] F. Solheim, J. Godwin, E. Westwater, Y. Han, S. Keihm, K. Marsh, and R. Ware, "Radiometric profiling of temperature, water vapor, and cloud liquid water using various inversion methods," *Radio Sci.*, vol. 33, no. 2, pp. 393–404, 1998.
- [6] SNOW-V10, Science and NOWcasting of Olympic Weather for Vancouver 2010, Accessed Sep. 3, 2010. [Online]. Available: <http://www.snow-v10.ca>
- [7] E. Campos, C. Doyle, and H. Winston, "Weather analysis for the 2010 Winter games," *Vaisala News*, vol. 182, pp. 16–17, 2010.
- [8] J. Mailhot, S. Belair, M. Charron, C. Doyle, P. Joe, M. Abrahamowicz, N. B. Bernier, B. Denis, A. Erfani, R. Frenette, A. Giguere, G. A. Isaac, N. McLennan, R. McTaggart-Cowan, J. Milbrandt, and L. Tong, "Environment Canada's experimental numerical weather prediction systems for the Vancouver 2010 Winter Olympic and Paralympic games," *Bull. Amer. Meteorol. Soc.*, vol. 11, pp. 1073–1085, 2010.
- [9] When Weather Matters: Science and Service to Meet Critical Societal Needs, Committee on Progress and Priorities of U.S. Weather Research and Research-to-Operations Activities, National Research Council, Washington, DC, ISBN: 978-0-309-15249-5, 2010.
- [10] Observing Weather and Climate From the Ground Up, A Nationwide Network of Networks, Committee on Developing Mesoscale Meteorological Observational Capabilities to Meet Multiple Needs, National Research Council, ISBN: 978-0-309-12986-2, 2009.
- [11] M. Decker, E. Westwater, and F. Guiraud, "Experimental evaluation of ground-based microwave sensing of atmospheric temperature and water vapour," *J. Appl. Meteor.*, vol. 17, no. 12, pp. 1788–1795, Dec. 1978.
- [12] A. Battaglia, E. Rustemeier, A. Tokay, U. Blahak, and C. Simmer, "PARSIVEL snow observations: A critical assessment," *J. Atmos. Ocean. Technol.*, vol. 27, no. 2, pp. 333–344, Feb. 2010.
- [13] B. E. Sheppard and P. I. Joe, "Performance of the Precipitation Occurrence Sensor System as a precipitation gauge," *J. Atmos. Ocean. Technol.*, vol. 25, no. 2, pp. 196–212, Feb. 2008.
- [14] C. D. Rodgers, *Inverse Methods for Atmospheric Sounding: Theory and Practice*. Singapore: World Scientific, 2000.
- [15] S. Albers, J. McGinley, D. Birkenheuer, and J. Smart, "The Local Analysis and Prediction System (LAPS): Analyses of clouds, precipitation, and temperature," *Weather Forecast.*, vol. 11, no. 3, pp. 273–287, Sep. 1996.
- [16] D. Cimini, R. Ware, G. Giuliani, J. Oremano, E. Campos, S. Albers, P. Joe, S. Koch, and S. Cober, "Boundary layer thermodynamic profiling using ground-based microwave radiometry and 1DVAR for nowcasting," in *Proc. ISARS*, Paris, France, Jun. 28–30, 2010.
- [17] J. Schroeder and E. Westwater, User's Guide to Microwave Radiative Transfer Software, NOAA Tech. Memo., ERL WPL-213, 1991.
- [18] S. Kneifel, U. Löhnert, A. Battaglia, S. Crewell, and D. Siebler, "Snow scattering signals in ground-based passive microwave radiometer measurements," *J. Geophys. Res.*, vol. 115, p. D16214, Aug. 2010, doi: 10.1029/2010JD013856.
- [19] J. C. Liljegren, S. A. Boukabara, K. Cady-Pereira, and S. A. Clough, "The effect of the half-width of the 22-GHz water vapor line on retrievals of temperature and water vapor profiles with a twelve-channel microwave radiometer," *IEEE Trans. Geosci. Remote Sens.*, vol. 43, no. 5, pp. 1102–1108, May 2005.
- [20] K. E. Cady-Pereira, M. Sheppard, D. Turner, E. Mlawer, S. Clough, and T. Wagner, "Improved daytime column integrated precipitable water vapor from Vaisala radiosonde humidity sensors," *J. Atmos. Ocean. Technol.*, vol. 25, no. 6, pp. 873–883, Jun. 2008.
- [21] P. Eriksson, C. Jimenez, and S. A. Buehler, "Qpack, a general tool for instrument simulation and retrieval work," *J. Quant. Spectrosc. Radiat. Transf.*, vol. 19, no. 1, pp. 47–64, Feb. 2005.
- [22] L. E. Johnson and B. G. Olsen, "Assessment of quantitative precipitation forecasts," *Weather Forecast.*, vol. 13, no. 1, pp. 75–83, Mar. 1998.
- [23] F. S. Marzano, M. Palmacci, D. Cimini, G. Giuliani, and J. F. Turk, "Multivariate statistical integration of satellite infrared and microwave radiometric measurements for rainfall retrieval at the geostationary scale," *IEEE Trans. Geosci. Remote Sens.*, vol. 42, no. 5, pp. 1018–1032, May 2004.
- [24] E. R. Westwater, "Ground-based microwave remote sensing of meteorological variables," in *Atmos. Remote Sens. Microw. Radiometry*, M. A. Janssen, Ed. New York: Wiley, 1993, pp. 145–213.
- [25] S. Crewell, K. Ebell, U. Löhnert, and D. D. Turner, "Can liquid water profiles be retrieved from passive microwave zenith observations?" *Geophys. Res. Lett.*, vol. 36, p. L06803, 2009, doi: 10.1029/2008GL036934.
- [26] V. Mattioli, P. Basili, S. Bonafoni, P. Ciotti, and E. Westwater, "Analysis and improvements of cloud models for propagation studies," *Radio Sci.*, vol. 44, p. RS2005, 2009.
- [27] A. Battaglia, P. Saavedra, T. Rose, and C. Simmer, "Rain observations by a multi-frequency dual polarized radiometer," *IEEE Geosci. Remote Sens. Lett.*, vol. 6, no. 2, pp. 354–358, Apr. 2009.
- [28] R. Kisler, NOAA NCEP Environ. Model. Center, Global Model. Branch, Accessed Sep. 1, 2010. [Online]. Available: <http://www.emc.ncep.noaa.gov/gmb/bkistler/>
- [29] S. Saha, S. Moorthi, H.-L. Pan, X. Wu, J. Wang, S. Nadiga, P. Tripp, R. Kistler, J. Woollen, D. Behringer, H. Liu, D. Stokes, R. Grumbine, G. Gayno, J. Wang, Y.-T. Hou, H.-Y. Chuang, H.-M. H. Juang, J. Sela, M. Iredell, R. Treadon, D. Kleist, P. V. Delst, D. Keyser, J. Derber, M. Ek, J. Meng, H. Wei, R. Yang, S. Lord, H. van den Dool, A. Kumar, W. Wang, C. Long, M. Chelliah, Y. Xue, B. Huang, J.-K. Schemm, W. Ebisuzaki, R. Lin, P. Xie, M. Chen, S. Zhou, W. Higgins, C.-Z. Zou, Q. Liu, Y. Chen, Y. Han, L. Cucurull, R. W. Reynolds, G. Rutledge, and M. Goldberg, "The NCEP climate forecast system reanalysis," *Bull. Amer. Meteorol. Soc.*, vol. 91, no. 8, pp. 1015–1057, 2010.



Domenico Cimini received the Laurea and Ph.D. degrees in physics from the University of L'Aquila, L'Aquila, Italy.

In 2004–2005, he was a Visiting Fellow at the Cooperative Institute for Research in Environmental Sciences, University of Colorado (CU), Boulder. He is currently with the Institute of Methodologies for Environmental Analysis (IMAA), Italian National Research Council (CNR), Tito Scalo, Italy. Since 2002, he has been with the Center of Excellence for Severe Weather Forecast (CETEMPS), University of

L'Aquila. Since 2006, he has been an Affiliate of the CU Center for Environmental Technology, Department of Electrical and Computer Engineering, CU, where he served as an Adjunct Professor in 2007.

Dr. Cimini was the recipient of the 2008 *Fondazione Ugo Bordononi Award* in memory of Prof. Giovanni D'Auria.



Graziano Giuliani received the Laurea degree in physics from the University of Rome "La Sapienza," Rome, Italy, in 1997.

He was with the Center of Excellence for Severe Weather Forecast (CETEMPS), University of L'Aquila, L'Aquila, Italy, as a Research Scientist until March 2011, when he joined the International Centre for Theoretical Physics, United Nations Educational, Scientific and Cultural Organization, Trieste, Italy, on Service Agreement. He has worked through the years for a number of Italian research and

service institutions on meteorology, climate, and high-performance computing fields.

Jeos Oreamuno, photograph and biography not available at the time of publication.

Paul Joe, photograph and biography not available at the time of publication.



Edwin Campos received the B.Sc. and Licentiate degrees in meteorology from the Regional Training Center of the World Meteorological Organization, Universidad de Costa Rica, San Jose, Costa Rica, in 1994 and 1996, respectively, and the M.Sc. and Ph.D. degrees in atmospheric science from McGill University, Montreal, ON, Canada, in 1998 and 2007, respectively.

He was a Weather Forecaster and a Lead Meteorologist with the Costa Rican Meteorological Service (in 1994–2002). He was also a Visiting Meteorologist at the Canadian Meteorological Centre (in August–December 1995); a

Visiting Scientist at the National Astronomy and Ionosphere Center Arecibo Observatory, Cornell University (in September–October 1998), Arecibo, Puerto Rico; a Visiting Meteorologist at the National Hurricane Center, National Oceanic and Atmospheric Administration (in August–September 1999), and an Undergraduate Meteorology Lecturer with the Universidad de Costa Rica (in 1999–2002). From 2007 to 2010, he was a Visiting Research Fellow with the Cloud Physics and Severe Weather Research Group, Environment Canada, supporting the Vancouver 2010 Olympic and Paralympic Winter Games. He is currently a Research Meteorologist with the Atmospheric Radiation Measurement (ARM) Climate Research Facility, Computing, Environment and Life Sciences Directorate, Argonne National Laboratory, Argonne, IL.

Dr. Campos is a member of the American Meteorological Society, the American Geophysical Union, and the Canadian Meteorological and Oceanographic Society.



Steven E. Koch received the B.S. and M.S. degrees in meteorology from the University of Wisconsin, Madison, and the Ph.D. degree in meteorology from The University of Oklahoma, Norman.

Recently, he resigned as the Director of the Global Systems Division, Earth Systems Research Laboratory, National Oceanic and Atmospheric Administration (NOAA), Boulder, CO. Prior to that, he was the Chief of the Forecast Research Division, NOAA's Forecast Systems, from 1993 to 2000, a tenured Associate Professor with North Carolina State University, Raleigh, and a Research Meteorologist with NASA/Goddard Space Flight Center, Greenbelt, MD, from 1980 to 1993. He is currently the Director of the National Severe Storms Laboratory, NOAA, Norman. His current professional activities include acting as an Adjunct Full Professor at several universities, as a Fellow of the American Meteorological Society, and as the Deputy Director of the NOAA/NCAR Developmental Testbed Center. He is the author or coauthor of 64 scientific articles in professional journals on subjects ranging from gravity wave and frontal dynamics to numerical prediction and dynamics of turbulence, satellite meteorology, mesometeorology, numerical weather prediction, data assimilation, mesoanalysis using remote sensing systems, scientific data visualization, and operational forecasting techniques.

Stewart Cober, photograph and biography not available at the time of publication.

Stewart Cober, photograph and biography not available at the time of publication.



Randolph "Stick" Ware received the Ph.D. degree in experimental nuclear physics from the University of Colorado, Boulder, in 1974.

He was the Director of GPS Science and Technology Program, University Corporation for Atmospheric Research, in 1998–2004 and the University NAVSTAR Consortium in 1985–1998; a Principal Investigator of the Global Positioning System/Meteorology Radio Occultation Satellite Program (precursor to COSMIC) in 1991–1995 and SuomiNet in 1999–2004; a Cooperative Institute for Research

in Environmental Sciences (CIRES) Fellow in 1985–1991; a U.S. Congressional Science Fellow in 1983–1984; a CIRES Research Scientist in 1979–1983; and a JILA (National Institute of Standards and Technology/University of Colorado) Postdoctoral Scientist in 1974–1978. He is currently the Founder and a Chief Scientist of Radiometrics Corporation, Boulder; a Visiting Scientist at the Mesoscale and Microscale Meteorology Division, National Center for Atmospheric Research, Boulder; and a Senior Associate Scientist with the CIRES (National Oceanic and Atmospheric Administration/University of Colorado). He is the Founder of Boulder Beer. He has authored or coauthored 80 peer-reviewed scientific articles and is the holder of 11 U.S. and international patents.



Ed Westwater (SM'91–F'01) received the B.A. degree in physics and mathematics from the Western State College of Colorado, Gunnison, in 1959 and the M.S. and Ph.D. degrees in physics from the University of Colorado (CU), Boulder, in 1962 and 1970, respectively.

He was with the U.S. Department of Commerce from 1960 to 1995. He retired in 2009 as a Research Professor with CU. He has been with Cooperative Institute for Research in Environmental Sciences, Boulder, since 1995, and joined Center for Environmental Technology, Electrical, Computer, and Energy Engineering, University of Colorado, Boulder, in 2006. He served as an Associate Editor of *Radio Science*. He has authored or coauthored more than 290 publications.

Dr. Westwater was the recipient of the 2003 Distinguished Achievement Award from the IEEE Geoscience and Remote Sensing Society and the 15th Vaisala Award from the World Meteorological Society in 2001. He is a member of the American Meteorological Society, the American Geophysical Union, and the Mathematical Association of America. He is the past Chairman of URSI Commission F. He presented the American Meteorological Society's Remote Sensing Lecture in 1997. He was an Associate Editor of the IEEE TRANSACTIONS ON GEOSCIENCE AND REMOTE SENSING (TGARS) and served as a Guest Editor of TGARS Special Issues devoted to the International Specialists Meeting on Microwave Radiometry and Remote Sensing Applications (MicroRad) in 2004, 2006, and 2008.

Steve Albers, photograph and biography not available at the time of publication.